World Academy of Science, Engineering and Technology
International Journal of Chemical and Molecular Engineering
Vol:8, No:11, 2014

Stabilization of Transition Metal Chromite Nanoparticles in Silica Matrix

Jiri Plocek, Petr Holec, Simona Kubickova, Barbara Pacakova, Irena Matulkova, Alice Mantlikova, Ivan Nemec, Daniel Niznansky, Jana Vejpravova

Abstract—This article presents summary on preparation and characterization of zinc, copper, cadmium and cobalt chromite nanocrystals, embedded in an amorphous silica matrix. The $ZnCr_2O_4/SiO_2$, $CuCr_2O_4/SiO_2$, $CdCr_2O_4/SiO_2$ and $CoCr_2O_4/SiO_2$ nanocomposites were prepared by a conventional sol-gel method under acid catalysis. Final heat treatment of the samples was carried out at temperatures in the range of $900-1200\,^{\circ}C$ to adjust the phase composition and the crystallite size, respectively. The resulting samples were characterized by Powder X-ray diffraction (PXRD), High Resolution Transmission Electron Microscopy (HRTEM), Raman/FTIR spectroscopy and magnetic measurements. Formation of the spinel phase was confirmed in all samples. The average size of the nanocrystals was determined from the PXRD data and by direct particle size observation on HRTEM; both results were correlated. The mean particle size (reviewed by HRTEM) was in the range from ~ 4 to 46 nm. The results showed that the sol-gel method can be effectively used for preparation of the spinel chromite nanoparticles embedded in the silica matrix and the particle size is driven by the type of the cation A^{2+} in the spinel structure and the temperature of the final heat treatment. Magnetic properties of the nanocrystals were found to be just moderately modified in comparison to the bulk phases.

Keywords—Chromite, Fourier transform infrared spectroscopy, agnetic properties, nanocomposites, Raman spectroscopy, Rietveld refinement, sol-gel method, spinel.

I. Introduction

CHROMITES with $A^{2+}Cr_2^{3+}O_4$ formula are binary oxides, where A^{2+} and Cr^{3+} are cations occupying tetrahedral (A) and octahedral (B) sites, respectively. The chromites are considered as materials with variety of potential applications ranging from high-temperature ceramics [1], catalysis [2], semiconductors [3]–[6] to electrochemical sensors [7].

At high-enough temperatures, the chromites crystallize in a cubic structure (space group *Fd-3m*), with 56 atoms per unit cell (Z = 8). The $3d^3$ electron configuration of Cr^{3+} is very stable because each of the t_{2g} energy level is singly occupied, so there is no tendency of site mixing or mixed valence. In the chromites with Jahn-Teller (JT) active A^{2+} cations, the collective JT distortions on the A-cations results in a reduction in symmetry from cubic *Fd-3m* to tetragonal *$I4_1$/amd* upon orbital ordering at the transition temperature. The magnetic ordering is therefore characteristic by a considerable spin frustration and strongly depend on the chemical order (the spinel inversion, oxygen deficit etc.) and on the cation site occupancy in the spinel structure [8] (diamagnetic, paramagnetic or JT active), respectively.

The zinc chromite is known as a frustrated antiferromagnet with a complex coplanar spin structure below the Neél temperature, $T_N = 12$ K [9] and it is arguably the most magnetically-frustrated system known so far. At room temperature, it has a cubic crystal structure where Cr^{3+} ions form a network of pyrochlore-like lattice [10]. The Curie-Weiss temperature is about 390 K, indicating strong antiferromagnetic frustration, yet chromium spins remain in a cooperative paramagnetic phase down to the T_N. There, a first-order phase transition from a cubic paramagnet to a tetragonal antiferromagnet signals the end of distinct spin and lattice degrees of freedom. It is a unique example of the so-called spin Jahn-Teller system [11].

The other example with a diamagnetic cation, the cadmium chromite exhibits an elliptical spiral magnetic structure below the $T_N = 7.8$ K and simultaneously reveals a dielectric anomaly at the T_N [12]. The $CdCr_2O_4$ also undergoes a spin-Peierls-like lattice distortion at the T_N [13], [14]. The lattice symmetry is lowered from cubic to tetragonal; the lattice is elongated along the c-axis, while it shrinks in the same direction in the $ZnCr_2O_4$. It is also surprising that the magnitude of the distortion is larger in the Zn compound with weaker magnetic interactions.

While less common, tetrahedral Cu^{2+} on the A site of the spinel network also displays JT activity, with the relatively high JT temperature, $T_{JT} = 830$ K, resulting in the tetragonal structure (space group *$I4_1$/amd*). This distortion lowers symmetry by compressing the tetrahedron and thereby breaking the degeneracy of the partially-occupied t_2 energy levels [15]. Magnetic properties of the copper chromite have been rarely investigated, it is reported as a hard ferromagnet with the Curie temperature, $T_C = 135$ K.

Cobalt chromite samples with magnetic Co^{2+} (d^7) cations develop below $T_C = 94$ K long-range ferrimagnetic order, and moreover exhibits a sharp phase transition at $T_S = 27$ K to the onset of long-range spiral magnetic order [16], [17]. Magneto-capacitive measurements show that the dielectric constant of $CoCr_2O_4$ couples to the spiral magnetic order parameter, but is insensitive to the ferrimagnetic spin component [18].

J.Plocek and P.Holec are with the Institute of Inorganic Chemistry, v.v.i., Academy of Sciences of the CR, 250 68 Rez, Czech Republic.

P.Holec, I.Matulkova, I.Nemec and D.Niznansky are with the Charles University Prague, Faculty of Science, Department of Inorganic Chemistry, Hlavova 2030, 128 40, Prague 2, Czech Republic.

S.Kubickova, B.Pacakova, A.Mantlikova and J.Vejpravova are with the Institute of Physics, v.v.i., Academy of Sciences of the CR, Na Slovance 2, 18221 Prague, Czech Republic (corresponding author J.Vejpravova to provide phone: +420-266-052-325; fax: +420-286-890-527; e-mail: vejpravo@fzu.cz).

As is known, the magnetic properties such as saturation magnetization, remanent magnetization and coercivity, respectively, depend strongly on the particles size and microstructure of the materials. In case of the spinel chromites, significant change of magnetic order and hence dielectric response is expected upon reduction of the particle size below a coherence length of the spiral component of the magnetic structure [17], [19]. Therefore it is important to use a proper technique by which both the size and the shape of particles can be well controlled. One of the ways to prepare the nanocrystals with the required properties represents the sol-gel method [20], [21]. The advantages of this method are namely a good homogeneity of the final materials, low temperatures of the treatment, and control of the particle size by final heat treatment. On the other hand, to stabilize a ternary spinel phase in silica matrix, which has an acidic nature, is a challenging task.

In this work we focused on optimization of the fabrication procedure in order to obtain single phase transition metal chromite nanoparticles, embedded in the silica matrix. The optimized samples were investigated by varied of experimental techniques and results of structure characterization and magnetic properties are presented. Moreover, the impact of the size reduction on magnetic order in selected ACr_2O_4 is also discussed.

II. Experimental

A. Materials Preparation

The conventional sol-gel method using TEOS, HNO_3 as an acid catalyst, formamide as a modifier, and methanol as a solvent, was used for preparation of the nanocomposites. The sol was prepared by dissolving of the corresponding amount of the $Cr(NO_3)_3 \cdot 9H_2O$ and the $Zn(NO_3)_2 \cdot 6H_2O$, $Cu(NO_3)_2 \cdot 3H_2O$, $Cd(NO_3)_2 \cdot 4H_2O$, or $Co(NO_3)_2 \cdot 6H_2O$, respectively, in methanol. The Si/Cr molar ratio was 5/1, which corresponds to the SiO_2/ACr_2O_4 (where A = Zn, Cu, Cd, and Co) molar ratio of 10/1. The gelation time was approximately 24 h at 40 °C. The samples were left 48 h for ageing. Then they were progressively dried at 40 °C for 2 days in flowing N_2-atmosphere. After drying, they were preheated first at 300 °C in a vacuum for 2 h and then at various temperatures (900, 1000, 1100, 1200 °C) under normal atmosphere. The samples were heated for two hours at the above-mentioned heating temperatures.

B. Materials Characterization

The final products were characterized at room temperature using the Bragg- Brentano geometry on a Philips X'pert PRO MPD X-ray diffraction system equipped with a ultra fast X'Celerator detector using Cu-anode (Cu K_α; $\lambda = 1.5418$ Å). The particle diameters (mean size of the coherently diffracting domain) and lattice parameters were obtained using the Rietveld refinement within the program FullProf software [22] where the instrumental broadening was eliminated by measuring the calibration standard (in our case, the LaB_6 was used).

The size and shape of prepared nanocomposites were analyzed on a HRTEM JEOL JEM 3010 (High-Resolution Transmission Electron Microscope). Particle size distribution was obtained by manual measurement and statistical evaluation of large-scale projected images. Elemental composition of nanoparticles was verified by EDS (Energy-dispersive X-ray spectroscopy) analysis.

The infrared spectra were recorded on a Thermo Scientific Nicolet 6700 FTIR spectrometer (2 cm^{-1} resolution, KBr beamsplitter, DTGS detector, Happ-Genzel apodization) in the 400 - 4000 cm^{-1} region using nujol mull (KBr windows) technique. The FAR IR spectra were recorded down to 50 cm^{-1} (4 cm^{-1} resolution, Solid SubstrateTM beamsplitter, DTGS detector, Happ-Genzel apodization) in PE pellets.

The Raman spectra were recorded on a Thermo Scientific DXR Raman Microscope interfaced to an Olympus microscope (objective 50x) in the 50 - 1900 cm^{-1} spectral region with ~ 3 cm^{-1} resolution. The power of frequency-stabilized single mode diode laser (780 nm) impinging on the sample was ranging from 1 to 4 mW. The spectrometer was calibrated by software-controlled calibration procedure using multiple neon emission lines (wavelength calibration), multiple polystyrene Raman bands (laser frequency calibration) and standardized white light sources (intensity calibration).

Magnetic properties were measured using a commercial 7 T - SQUID magnetometer (MPMS by Quantum Design) in the temperature range 2 - 350 K.

III. Results and Discussion

A. Powder X-ray Diffraction Measurement

The PXRD measurements were carried out on all samples and are shown in Fig. 1. Phase compositions (of selected samples) are summarized in the Table I. All samples contained spinel phase, together with the other impurity phases in some cases, as will be discussed further. In some samples, the shape of the spinel phase diffraction peaks with the steep Lorentzian like and the broad Gausian- like components was detected, suggesting that the diffraction pattern is the superposition of two patterns representing two different size fractions of particles within the spinel phase. In case of unimodal particle size distribution, the crystallite size could be determined by analysis of the broadening of diffraction peaks using the well-known Scherrer equation [23] in the simplest approximation. Because of the complexity of the diffraction patterns, this approach would be absolutely inappropriate and would give average weighted diameter of both phases of different particle size. Therefore, the Rietveld refinement has been used for the calculations of the proper crystallite sizes. The results were in accordance with results obtained from direct particles observation by HRTEM. An overview of the chromite particle size, the phase composition of the samples and the determined lattice parameters is written in the Table I. The lattice parameters, *a* are in good agreement with those observed by other authors [24], [25].

TABLE I
THE SAMPLES WITH THEIR FINAL PREPARATION TEMPERATURES AND THEIR BASIC CHARACTERISTICS

Sample	Phase Comp.[a]	d_{HRTEM}[b] (nm)	d_{PXRD}[c] (nm)	Space Group	a[d] (Å)
$ZnCr_2O_4/SiO_2$-900 °C	$ZnCr_2O_4$	-	19.2	-	-
	Cr_2O_3	-	-	-	-
	(ZnO)	-	-	-	-
$ZnCr_2O_4/SiO_2$-1000 °C	$ZnCr_2O_4$	9; (11.2)	9.6	Fd-3m	8.3263
	Cr_2O_3	-	-	-	-
$ZnCr_2O_4/SiO_2$-1100 °C	$ZnCr_2O_4$	11, 21; (15.0)	10.2; 20.1	Fd-3m	8.3354
$CdCr_2O_4/SiO_2$-900 °C	Cr_2O_3	-	-	-	-
	$CdCr_2O_4$	-	-	-	-
	SiO_2 α-quartz	-	-	-	-
	$CdSiO_3$	-	-	-	-
$CdCr_2O_4/SiO_2$-1000 °C	$CdCr_2O_4$	-	15.0	Fd-3m	8.5978
	Cr_2O_3	-	-	-	-
	(SiO_2 α-quartz)	-	-	-	-
	(SiO_2 cristobalite)	-	-	-	-
$CdCr_2O_4/SiO_2$-1100 °C	$CdCr_2O_4$	7.5, 32.5, 87.5; (24.2)	38.9	Fd-3m	8.5978
	SiO_2 cristobalite	-	-	-	-
$CdCr_2O_4/SiO_2$-1200 °C	$CdCr_2O_4$	-	28.5	Fd-3m	8.5978
	SiO_2 cristobalite	-	-	-	-
	Cr_2O_3	-	-	-	-
$CoCr_2O_4/SiO_2$-900 °C	Cr_2O_3	-	-	-	-
	$CoCr_2O_4$	-	-	-	-
$CoCr_2O_4/SiO_2$-1000 °C	$CoCr_2O_4$	5, 25; (8.4)	5.1; 25.2	Fd-3m	8.3311, 8.2394[e]
$CoCr_2O_4/SiO_2$-1100 °C	$CoCr_2O_4$	7; (6.9)	6.0; 45.8	Fd-3m	8.3338, 8.3244[e]
$CuCr_2O_4/SiO_2$-900 °C	$CuCr_2O_4$	-	-	-	-
	Cr_2O_3	-	-	-	-
	$CuCrO_2$	-	-	-	-
$CuCr_2O_4/SiO_2$-1000 °C	$CuCr_2O_4$	9, 21; (9.3)	28	I 4_1/amd	a=6.0301, c = 7.8038
	Cr_2O_3	-	-	-	-
$CuCr_2O_4/SiO_2$-1100 °C	$CuCr_2O_4$	-	-	-	-
	SiO_2 cristobalite	-	-	-	-
	Cr_2O_3	-	-	-	-
	$CuCrO_2$	-	-	-	-

[a] Phase composition of prepared samples ordered with decreasing content; in parenthesis phases with trace amount are mentioned.
[b] d_{HRTEM} are maxima (modes) of particle size distributions determined by HRTEM; in parenthesis the mean chromite particle size is shown.
[c] d_{PXRD} are chromite particle sizes determined from PXRD using the Rietveld refinement.
[d] a denotes lattice parameters of chromite nanocrystals.
[e] denotes two different a-parameters which are corresponding to two different particles with different particle sizes.
Note: The sign '-' means that the value was not measured or calculated.

The analysis of the data demonstrated that the samples that contain spinel as the single phase were the $ZnCr_2O_4/SiO_2$-1100 °C, $CoCr_2O_4/SiO_2$-1000 °C and the $CoCr_2O_4/SiO_2$-1100 °C samples. In the other samples, even with the spinel as the major phase, the presence of other metal oxides and/or the crystalline SiO_2 was detected. The content of the spinel phase increases with increasing annealing temperature up to 1100 °C, and further decomposition for the sample annealed at higher temperature (the $CdCr_2O_4/SiO_2$-1200 °C sample) was observed. The SiO_2 remained amorphous for all Zn, Co and Cu samples except the $CuCr_2O_4/SiO_2$-1100 °C. In case of the Cd samples, the SiO_2 was crystalline, with evident transformation from the α-quartz phase to the α-cristobalite at 1100 °C. The 1100 °C

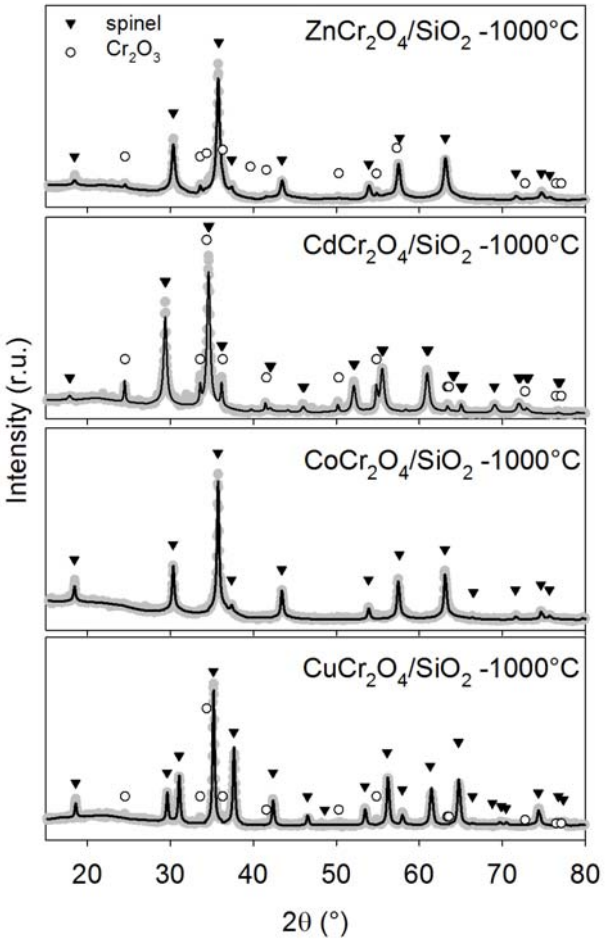

Fig. 1. The Powder X-ray diffraction paterns of the $ZnCr_2O_4/SiO_2$-1000 °C, $CdCr_2O_4/SiO_2$-1000 °C, $CoCr_2O_4/SiO_2$-1000 °C and $CuCr_2O_4/SiO_2$-1000 °C samples with the assingment of the diffraction peaks to the corresponding phases.

seems to be an ideal temperature for the formation of the single-phases chromites in the case of the Zn^{2+}, Co^{2+} and Cd^{2+} ions, respectively, while the highest amount of the Cu^{2+} and chromites was obtained by annealing the samples at 1000 °C, however a nonegligible amount of chromite oxide was also detected.

The analysis of the particle size confirmed increase of the size with increasing annealing temperature, as has been anticipated. The smaller particle size in case of the $CdCr_2O_4/SiO_2$-1200 °C sample in comparison with the samples annealed at lower temperature can be explained by the raised decomposition. The cobalt, zinc, and cadmium chromite nanoparticles exhibited at the room temperature the cubic structure. The only spinel crystallizing in the tetragonally distorted spinel phase as one of many examples of the Jahn-Teller effect was the Cu chromite.

The results of the PXRD analysis suggest, that the spinel chromite phase with Zn^{2+}, Cu^{2+}, Cd^{2+} and Co^{2+}, respectively, can be obtained as nanoparticles embedded in the silica matrix, regardless potential A^{2+} cation interaction with the silica matrix. The silica matrix behaves as a strong Lewis acid, which usually reacts with A^{2+} ions. Therefore, the metal silicates are expected to appear. Nevertheless, the spinel chromites are formed as a kinetically preferred form in our systems. Silicates were observed as a minority phase only in samples with cadmium (the most basic), and their amount varied depending on the heat treatment, with the preferential abundance at low temperature.

B. HRTEM observation

In order to give the complete information about the crystallite size and morphology, the detailed HRTEM investigation of selected nanocomposite samples was performed. The mean particle size in each sample was evaluated from several different images by statistical analysis of diameter of about 100 - 300 nanoparticles. For all HRTEM images, the dark parts represent the chromite nanocrystals (or crystalline oxide phases) and bright parts correspond to the amorphous silica matrix. In Fig. 2, the HRTEM images of the $ZnCr_2O_4/SiO_2$ samples annealed at 1000 and 1100 °C, $CdCr_2O_4/SiO_2$ annealed at 1100 °C, $CoCr_2O_4/SiO_2$ annealed at 1000 and 1100 °C and $CuCr_2O_4/SiO_2$ annealed at 1000 °C are depicted. Generally, the chromite particles are in all the samples more or less of spherical shape, as has been also suggested by PXRD measurements, where no shape anisotropy has been observed. The histograms with depicted particle size distributions are placed below the HRTEM images. There is an apparent wide and unsymmetrical particle size distribution, hence the maximum at particle size distribution curve (statistical mode) is more significant than usually used mean of the particle size value. There are also observable two maxima in some cases distribution is bimodal. Both type of the particle diameters, mode and mean, are depicted in the Table I.

As can be seen from the distribution of the particle size depicted in Fig. 2, the zinc nanocomposites heated at 1000 °C show a mode of particle size of 9 nm, whereas the zinc nanocomposites heated at 1100 °C show bimodal distribution with maxima at 11 and 21 nm, respectively. Particle size distribution of cadmium nanocomposite heated at 1100 °C is trimodal with observed maxima around 7.5, 32.5, and 87.5 nm, but the maximum at 32.5 nm is not so clear due to relatively small statistical ensemble. The particles of the cobalt chromite are very well defined and they did not exhibit a diffused appearance suggesting insufficient crystallinity. The modes of particle sizes of the $CoCr_2O_4$ nanocrystals treated at 1000 °C were found to be 5 and 25 nm. The particle size of the sample heated at 1100 °C moderately increased with increasing temperature as expected, and was determined as 7 nm. The HRTEM result for the $CuCr_2O_4/SiO_2$ sample annealed at 1000 °C is shown in Fig. 2. The maxima at particle size distribution of this spinel phase treated at 1000 °C were observed at 9 and 21 nm. The results of the observation particle size using HRTEM are in a good correspondence with the results obtained by analysis of PXRD data.

Generally, in case of a broad and multimodal particle size distributions, it is necessary to consider that the statistical processing of the HRTEM images is calculated by means of

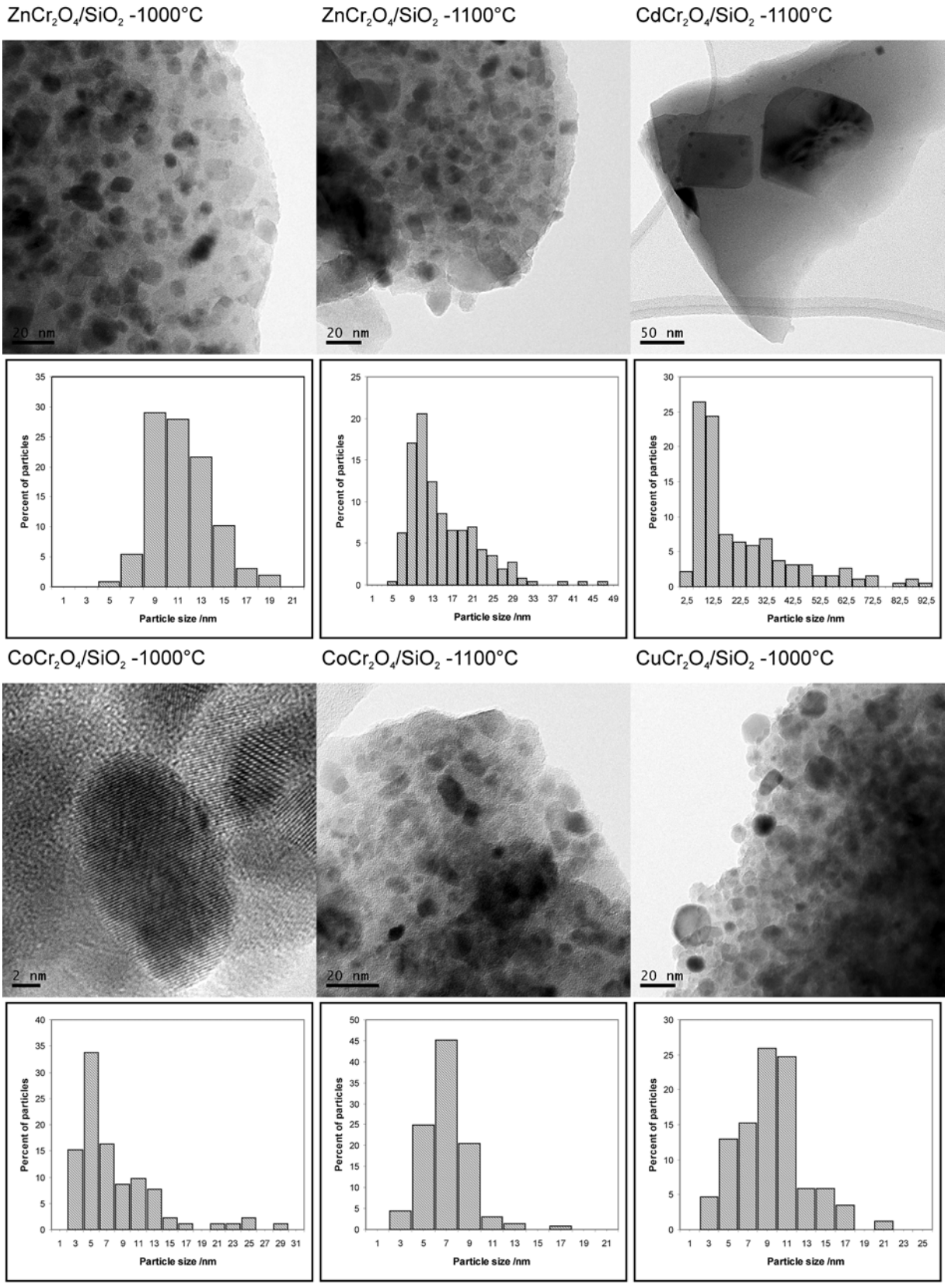

Fig. 2. The HRTEM images and the distribution of particle sizes of the $ZnCr_2O_4/SiO_2$ samples heated at 1000 and 1100 °C, $CdCr_2O_4/SiO_2$ sample heated at 1100 °C, $CoCr_2O_4/SiO_2$ samples heated at 1000 and 1100 °C, and the $CuCr_2O_4/SiO_2$ sample heated at 1000 °C.

particle diameter (1D characteristics of particles), whereas the PXRD reflects volume of the coherently scattering domain, and therefore it considers 3D characteristics of the particles. Particle size distribution evaluated by using the PXRD compared to the HRTEM, emphasizes amount of the fraction with large particles compared to the fraction with small particles in ratio of third powers of their dimensions. This is also the reason why some size fractions of the particles may not be observable by one of the methods.

C. IR and Raman Spectroscopy

The vibrational spectra of ACr_2O_4/SiO_2 (A = Zn, Cu, Cd, Co) nanocomposites were studied for the first time. The nanocomposites with highest chromite content (according to PXRD results) were selected for this study, namely the $ZnCr_2O_4/SiO_2$-1100 °C, $CuCr_2O_4/SiO_2$-1000 °C, $CoCr_2O_4/SiO_2$-1100 °C and $CdCr_2O_4/SiO_2$-1200 °C samples. The spectra recorded at room temperature are depicted in Fig. 3 (Raman spectra) and observed maxima are presented in Table II. The assignment of the observed bands (see Table II) reflects previous papers concerning the vibrational spectra of transition metals chromites [26]–[33]. This assignment is based on chromites belonging to the normal cubic II-III spinels with space group *Fd-3m* (O_h^7) for which group theoretical treatment yields following vibrational representations:

$$A_{1g} + E_g + F_{1g} + 3F_{2g} + 2A_{2u} + 2E_u + 4F_{1u} + 2F_{2u}.$$

The A_{1g}, E_g and three F_{2g} modes are Raman active while four F_{1u} modes are IR active. The potential lowering of the cubic O_h symmetry to tetragonal D_{4h} symmetry, which can occur due to eventual Jahn-Teller effect, is connected with splitting of triply degenerate modes F_{1u} (to A_{2u} and E_u) and F_{2g} (to B_{2g} and E_g), and of doubly degenerate mode E_g (to A_{1g} and B_{1g}).

The vibrational manifestations of $CoCr_2O_4/SiO_2$ nanocomposites are fully in accord with the expected presence of cobalt chromite with cubic symmetry. Very similar is the situation concerning $ZnCr_2O_4/SiO_2$ nanocomposites with exception of the absence of the weak E_g mode in the Raman spectra. The Raman spectra of the $CdCr_2O_4/SiO_2$ nanocomposites confirm the presence of cubic cadmium chromite in examined samples, as is consistent with the PXRD analysis. However; the recorded spectra were complicated by the presence of other nanocrystalline phases as chromium(III) oxide (bands at ca. 300, 350, 525, 550 and 610 cm^{-1}) and especially cristobalite (bands at ca. 225 and 410 cm^{-1}). The absence of A_{1g} mode is in accord with its very low intensity in Raman spectrum of bulk $CdCr_2O_4$ crystals [17]. The infrared spectra of $CdCr_2O_4/SiO_2$ nanocomposites exhibit only strong absorption bands of the cristobalite phase.

The vibrational spectra of the $CuCr_2O_4/SiO_2$ nanocomposites contain much higher number of the $CuCr_2O_4$ modes compared to other prepared chromites. The similar character of the spectra was observed also for bulk $CuCr_2O_4$ samples [18] and can be explained by Jahn-Teller effect of Cu(II) ions leading to lowering of lattice symmetry [16]. The observed bands can be assigned to splitting of F_{1u} (4) mode (IR bands at 116, 131 and 187 cm^{-1}), F_{2g} (3) mode (Raman bands at 120 and 186 cm^{-1}), F_{2g} (1) mode (Raman bands at 583 and 621 cm^{-1}) and F_{1u} (1) mode (IR bands at 568 and 608 cm^{-1}). The assignment of Raman bands in 400 - 560 cm^{-1} region is complicated by the overlapping of splitted F_{2g} (2) modes with E_g modes, which is associated with the changes of bands intensity (probably in terms of new A_{1g} mode formation). Expected splitting of IR active F_{1u} (2) mode was not recorded due to strong absorption of silica matrix. Observed level of above-mentioned splitting of degenerate modes indicates most likely tetragonal symmetry of prepared copper chromite [18], which is consistent with the PXRD observation.

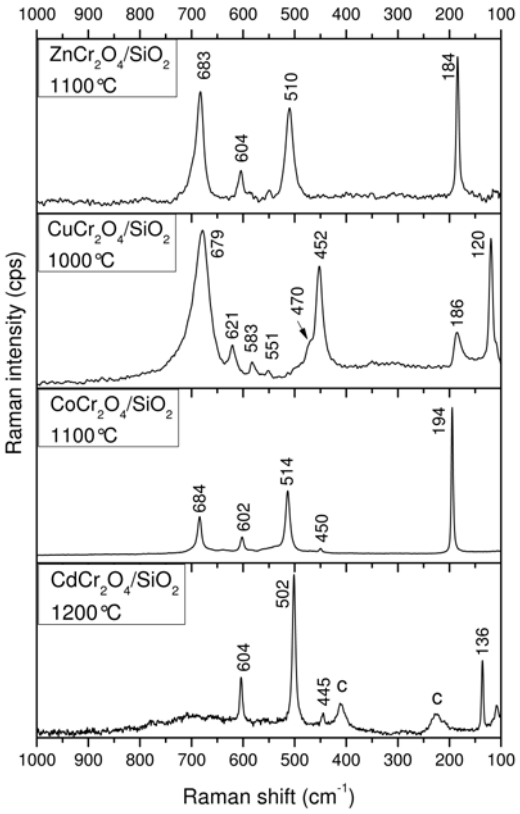

Fig. 3. The Raman spectra of the $ZnCr_2O_4/SiO_2$-1100 °C, $CuCr_2O_4/SiO_2$-1000 °C, $CoCr_2O_4/SiO_2$-1100 °C and $CdCr_2O_4/SiO_2$-1200 °C samples. The letter C denotes cristobalite bands.

D. Magnetic Properties

Results of magnetic measurements of the single-phase chromite nanocomposites are shown in Fig. 4 and 5. For the Zn-containing nanocomposites annealed at 1000 °C, the low-field magnetization, recorded in the zero field-cooled (ZFC) and field-cooled (FC) regime is almost identical. Both curves show a single anomaly at $T_N^* = 12.5$ K, which corresponds exactly to the Neél temperature of the bulk $ZnCr_2O_4$. The T_N^* shows a negligible temperature shift ($T_N^* = 12.0$ K) with applied field of 5 T, in consistency with

TABLE II
THE ASSIGNMENT OF THE VIBRATIONAL BANDS OF THE PREPARED TRANSITION METAL CHROMITE NANOPARTICLES EMBEDDED IN THE SILICA MATRIX.

$ZnCr_2O_4/SiO_2$-1100 °C		$CuCr_2O_4/SiO_2$-1000 °C		$CoCr_2O_4/SiO_2$-1100 °C		$CdCr_2O_4/SiO_2$-1200 °C	Symmetry
Raman (cm^{-1})	FTIR (cm^{-1})	Raman (cm^{-1})	FTIR (cm^{-1})	Raman (cm^{-1})	FTIR (cm^{-1})	Raman (cm^{-1})	
-	-	-	116 m	-	-	-	F_{1u} (4)
-	-	120 s	-	-	-	-	F_{2g} (3)
-	-	-	131 m	-	-	-	F_{1u} (4)
184 s	-	186 m	-	194 vs	-	136 m	F_{2g} (3)
-	186 s	-	187 m	-	197 s	-	F_{1u} (4)
-	364 w	-	367 w	-	373 w	-	F_{1u} (3)
-	-	-	-	450 vw	-	445 w	E_g
-	-	452 s	-	-	-	-	F_{2g} (3), E_g
-	-	470 sh	-	-	-	-	F_{2g} (3), E_g
-	544 m	-	n.o.[a]	-	532 m	-	F_{1u} (2)
510 s	-	551 w	-	514 s	-	502 s	F_{2g} (2)
-		583 w	-	-	-	-	F_{2g} (1)
604 m	-	621 m	-	602 w	-	604 m	F_{2g} (1)
-	-	-	568 m	-	-	-	F_{1u} (1)
-	632 m	-	608 m	-	627 m	-	F_{1u} (1)
683 s	-	679 s	-	684 m	-	-	A_{1g}

[a] Abbreviation "n.o." denotes expected vibrational bands, which were not observed due to silica matrix.

the character of the magnetization isotherm recorded at 2 K (inset of the Fig. 4), suggesting lack of any field-induced magnetic phase transition up to 5 T. A simple analysis of the high-temperature part of the magnetic susceptibility by means of the Curie-Weiss law yields the value of the paramagnetic Curie temperature, $\theta_P \sim$ - 138 K, which is considerably reduced in comparison to the bulk value, θ_P^{bulk} = - 380 K. The observed reduction of the θ_P can be interpreted as a consequence of the structure disorder, mostly in the nanoparticle shells, where the symmetry condition for the magnetic geometric frustration is removed. It is evident, that for the magnetic properties of the Zn-chromite nanocrystals embedded in the silica matrix with particle size of about 20 nm are not much modified.

The temperature dependence of the low-field ZFC magnetization of the $CdCr_2O_4$ nanocomposite shows a broad maximum at $\sim T_m = 60$ K, followed by a steep increase of the magnetization on cooling. The FC curve exhibits, on contrary, a paramagnetic-like trend and deviates from the ZFC curve at a irreversibility-like temperature $T_{irr} = 80$ K. The 1 T-curve is of Curie-Weiss character with the paramagnetic Curie temperature, $\theta_P \sim$ - 75 K. The magnetization isotherm recorded at 2 K exhibits a moderate coercivity value, $H_C = 0.01$ T, and can be effectively decomposed to a ferromagnetic-like and linear component. While the θ_P value corresponds well to the bulk ($\theta_P^{bulk} \sim$ - 70 K), the magnetic order in the nanocrystals is significantly different in comparison to the bulk material. The bulk $CdCr_2O_4$ orders antiferromagnetically at ~ 8 K and undergoes several magnetic phase transitions to the field-induced ferromagnetic state in high magnetic fields ($B > 25$ T). In the 39 nm nanocrystals, there is no evidence of the AF order. The anomaly at the $T_m = 60$ K can be attributed to the order of a fraction of the spins in a nanocrystal. As evidenced by the confrontation of the XRD and HRTEM results, the nanocrystals appears to be disordered with considerably large non-crystalline shell, therefore a spin-glass like order of the spins in the shell fraction may form, and also the AF order can be suppressed. The observation of the non-zero coercivity supports this scenario, on the other hand the linear contribution to the magnetization isotherm at 2 K cannot be simply explained, the best possible interpretation so far is the surface spin phenomenon as in case of the $ZnCr_2O_4$ nanocomposites.

For the $CuCr_2O_4$ nanocomposite, the temperature dependence of the low-field ZFC and FC magnetization, respectively bifurcate at $T_C = 150$ K, and additional broad maximum appears at $T_m \sim 30$ K, as demonstrated in the Fig. 5. The T_C roughly corresponds to the ordering temperature of the bulk $CuCr_2O_4$, similarly as reported in $MnCr_2O_4$ nanoparticles [19], the ordering temperature can be enhanced with the size reduction. However, the two other anomalies are of unclear origin. The character of the 30 K-maximum on the ZFC curve resembles that of a superparamagnetic system with medium particle size distribution. The saturation of the low-field FC curve can be viewed as a superposition of the ferromagnetic-like component coming from the regular order (at the $T^* = 150$ K) and a component of the SPM fraction with inter-particle interaction, as the curve changes its slope roughly at 30 K. The temperature dependencies of the magnetization recorded at higher magnetic fields (not shown) show a steep increase at the T_C, however

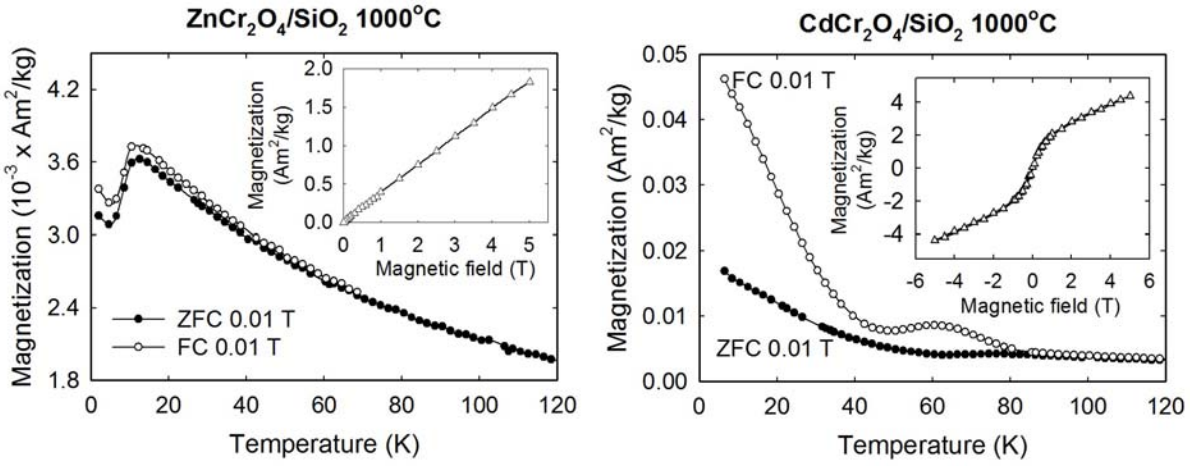

Fig. 4. Temperature dependence of zero field cooled (ZFC) and field cooled (FC) magnetization at magnetic field of 0.01 T for the $ZnCr_2O_4/SiO_2$ and $CdCr_2O_4/SiO_2$ samples annealed at 1000 °C. The insets show hysteresis loops recorded at 2 K.

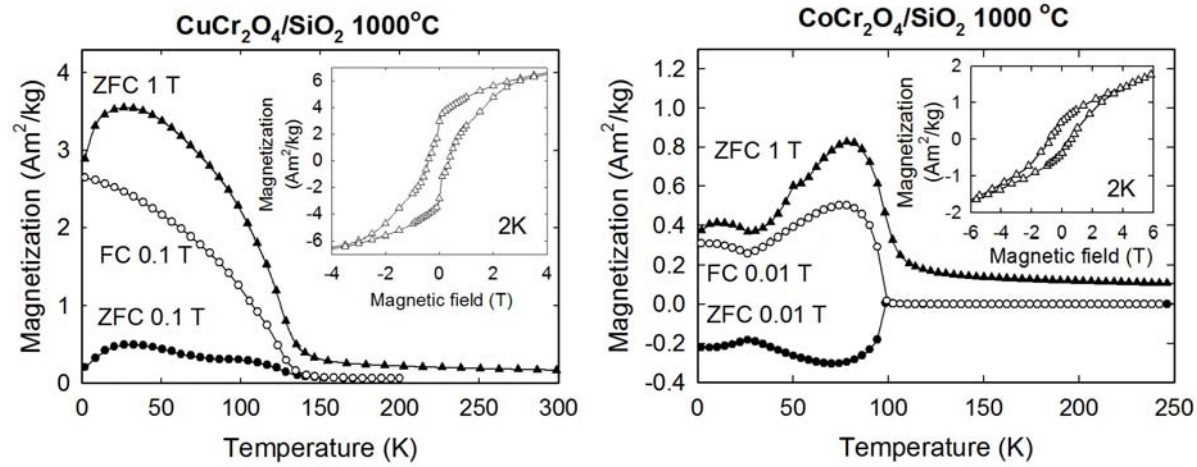

Fig. 5. Temperature dependence of zero field cooled (ZFC) and field cooled (FC) magnetization at magnetic field of 0.01 T , and ZFC magnetization at 1 T for the $CuCr_2O_4/SiO_2$ and $CoCr_2O_4/SiO_2$ samples annealed at 1000 °C. The insets show hysteresis loops recorded at 2 K.

the anomaly at 30 K is suppressed at 4 T. The observed paramagnetic Curie temperature, $\theta_P \sim -23$ K, estimated form the high-temperature part of the magnetic susceptibility, which contains contributions of the Cu and Cr sublattices, just signalizes, that the antiferromagnetic exchange path is dominant in the system. An additional minority feature can be observed at ~ 100 K on the low-field ZFC curve. It could be attributed to an additional order-to-order magnetic phase transition, however, there are no magnetization data available down to low temperatures on a bulk compound to support or exclude this interpretation. Moreover, the anomaly is completely suppressed in higher magnetic fields; therefore it can originate from a tiny amount of a magnetic impurity. The hysteresis loop recorded at 2 K shows a tiny necking, which can be interpreted as a superposition of the two phases with slightly different magnetic hardness. It closes at ~ 3 T, in consistency with the temperature dependence of magnetization, and the coercivity values is about 0.4 T at 2 K. This observation rather well support the fact, that part of the sample (potentially the core of the nanocrystals) behaves more-or-less like a bulk material, while the rest of the sample (the disordered shells of the nanocrystals) exhibit SPM-like phenomena modified by inter-particle interaction.

The temperature dependence of magnetization of the $CoCr_2O_4$ nanocomposite, shown in the Fig. 5, is characteristic with a series of anomalies at the temperatures almost corresponding to the bulk sample: $T_C = 99$ K and $T_S = 26$ K. The anomaly related to the so-called lock-in temperature ($T_f = 14$ K in bulk) [34] was not detected. A considerably large negative paramagnetic Curie temperature, $\theta_P \sim -86$ K, estimated form the high-temperature part of the magnetic susceptibility, was observed, pointing to AF interactions in the system. The hysteresis loop at 2 K (inset of the Fig. 5) shows a similar character as in case of the $CuCr_2O_4$, the coercivity is about 0.6 T. As evidenced by the obtained results, the behavior of the $CoCr_2O_4$ nanocrystals is not

much modified in comparison to the bulk material. It is in consistency with the assumption, that collapse of the magnetic order in the ground state magnetic phase is connected with size reduction below the coherence length of the conical component (~ 3 nm), which is not the case in our sample. The lack of the T_f - related anomaly can be, however, tentatively attributed to the size effect; as this temperature corresponds to stabilization of the canting angle in the ground state magnetic structure, the canting can either freezes already at the T_S or there is no equilibrium canting angle down to low temperatures in the nanocomposite.

IV. Conclusion

In spite of the acidic character of the silica matrix, the spinel phase is formed in the $ZnCr_2O_4/SiO_2$, $CdCr_2O_4/SiO_2$, $CuCr_2O_4/SiO_2$ and $CoCr_2O_4/SiO_2$ nanocomposites and these phases are do not transform to silicates up to 1100 °C. The amorphous silica matrix undergoes recrystallization to the cristobalite phase, depending on the A^{2+} cation. In presence of the copper cation (2+), it transforms at 1100 °C while for the cadmium-containing sample the silica matrix re-crystallizes already at 900 °C. At the zinc and cobalt samples remained the silica matrix amorphous up to the highest firing temperatures. It can be concluded that the type of the divalent cation significantly affects the crystallization of the amorphous silica matrix. The HRTEM observation, in accordance to the PXRD measurement, revealed uni-, bi- , and trimodal particle size distributions depending on the A^{2+} cation and annealing temperature. Optimal preparation temperature for chromite nanocomposites is 1000 °C for copper chromite, 1100 °C for zinc and cadmium chromites, and temperatures in the range from 1000 to 1100 °C for cobalt chromite.

Magnetic properties of the nanocomposites were only moderately modified with respect to the bulk phases. The most striking is the suppression of the antiferromagnetic order in the cadmium chromite sample and lack of the lock-in temperature in the cobalt chromite sample.

Acknowledgment

The authors thank for financial support of the Grant Agency of the Czech Republic, the project no. P108/10/1250.

References

[1] B. N. Kim, K. Hiraga, K. Merita and Y. Sakka, "A high-strain-rate superplastic ceramic", *Nature*, vol. 413, pp. 288-291, July 2001.

[2] K. Zakrzewska, "Mixed oxides as gas sensors", *Thin Solid Films*, vol. 391, pp. 229-239, July 2001.

[3] A. Galdikas, Z. Martunas and A. Setkus, "SnInO-based chlorine gas sensor", *Sens. Actuators B*, vol. 7, pp. 633-636, March 1992.

[4] D. H. Dawson and D. E. Williams, "Gas-sensitive resistors: surface interaction of chlorine with semiconducting oxides", *J. Mater. Chem.*, vol. 6, pp. 409-414, 1996.

[5] C. V. Gropal Reddy, S. V. Manorama and V. J. Rao, "Semiconducting gas sensor for chlorine based on inverse spinel nickel ferrite", *Sens. Actuators B*, vol. 55, pp. 90-95, Apr. 1999.

[6] J. Tamaki, C. Naruo, Y. Yamamoto and M. Matsuoka, "Sensing properties to dilute chlorine gas of indium oxide based thin film sensors prepared by electron beam evaporation", *Sens. Actuators B*, vol. 83, pp. 190-194, March 2002.

[7] H. Aono, F. Sugimoto, Y. Mori and Y. Okajima, "Cl_2 gas sensor using $BaCl_2$-KCl solid-electrolyte prepared by melting method", *Chem. Lett.*, vol. 6, pp. 1039-1042, 1993.

[8] X. Niu, D. Weiping and D. Weiumin, "Preparation and gas sensing properties of ZnM_2O_4 (M = Fe, Co, Cr)", *Sens. Actuators B*, vol. 99, pp. 405-409, May 2004.

[9] S. Ji, S.-H. Lee, C. Broholm, T. Y. Koo, W. Ratcliff, S.-W. Cheong et al., "Spin-lattice order in frustrated $ZnCr_2O_4$", *Phys. Rev. Lett.*, vol. 103, pp. 037201, July 2009.

[10] S.-H. Lee, C. Broholm, W. Ratcliff, G. Gasparovic, Q. Huang, T. H. Kim et al., "Emergent excitations in a geometrically frustrated magnet", *Nature*, vol. 418, pp. 856-858, July 2002.

[11] S.-H. Lee, C. Broholm, T. H. Kim, W. Ratcliff and S.-W. Cheong, "Local spin resonance and spin-peierls-like phase transition in a geometrically frustrated antiferromagnet", *Phys. Rev. Lett.*, vol. 84, pp. 3718-3721, Apr. 2000.

[12] M. Matsuda, "Magnetic structure of a frustrated antiferromagnetic spinel $CdCr_2O_4$studied by spherical neutron polarimetry", *Phys. B*, vol. 397, pp. 7-10, July 2007.

[13] Y. Yamashita and K. Ueda, "Spin-driven Jahn-Teller distortion in a pyrochlore system", *Phys. Rev. Lett.*, vol. 85, pp. 4960-4963, Dec. 2000.

[14] J.-H. Chung, M. Matsuda, S.-H. Lee, K. Kakurai, H. Ueda et al., "Statics and dynamics of incommensurate spin order in a geometrically frustrated antiferromagnet $CdCr_2O_4$", *Phys. Rev. Lett.*, vol. 95, pp. 247204, Dec. 2005.

[15] M. Gerloch, "The sense of Jahn-Teller distortions in octahedral copper(II) and other transition-metal complexes", *Inorg. Chem.*, vol. 20, pp. 638-640, Febr. 1981.

[16] N. Menyuk, K. Dwight and A. Wold, "Ferrimagnetic spiral configurations in cobalt chromite", *J. Phys. France*, vol. 25, pp. 528-536, May 1964.

[17] K. Tomiyasu, J. Fukunaga, and H. Suzuki, "Magnetic short-range order and reentrant-spin-glass-like behavior in $CoCr_2O_4$ and $MnCr_2O_4$ by means of neutron scattering and magnetization measurements", *Phys. Rev. B*, vol. 70, pp. 214434, Dec. 2004.

[18] G. Lawes, B. Melot, K. Page, C Ederer, M. A. Hayward, Th. Proffen et al., "Dielectric anomalies and spiral magnetic order in $CoCr_2O_4$" *Phys. Rev. B*, vol. 74, pp. 024413, July 2006.

[19] R. N. Bhowmik, R. Ranganathan and R. Nagarajan, "Lattice expansion and noncollinear to collinear ferrimagnetic order in a $MnCr_2O_4$ nanoparticle", *Phys. Rev. B*, vol. 73, pp. 144413, Apr. 2006.

[20] J. Plocek, A. Hutlova, D. Niznansky, J. Bursik, J. L. Rehspringer and Z. Micka, "Preparation of $CuFe_2O_4/SiO_2$ Nanocomposite by Sol-Gel Method", *Mater. Sci.-Poland*, vol. 23, pp. 697-705, 2005.

[21] J. Plocek, A. Hutlova, D. Niznansky, J. Bursik, J. L. Rehspringer and Z. Micka, "Preparation of $ZnFe_2O_4/SiO_2$ and $CdFe_2O_4/SiO_2$ nanocomposites by solgel method", *J. Non-Cryst. Solids*, vol. 315, pp. 70-76, Jan. 2003.

[22] J. Rodriguez-Carvajal, *FullProf User's Guide Manual*, France: CEA-CRNS, 2000.

[23] P. Scherrer, "Bestimmung der Größe und der inneren Struktur von Kolloidteilchen mittels Röntgenstrahlen", *Nachr. Ges. Wiss. Göttingen*, vol. 2, pp. 98-100, 1918.

[24] P. García Fasado and I. Raisnes, "Preparation and crystal data of the spinel series $Co_{1+2s}Cr_{2-3s}Sb_sO_4$ ($O \leq s \leq 3/2$)", *Polyhedron*, vol. 5, pp. 787-789, 1986.

[25] D. Levy, V. Diella, A. Pavese, M. Diapiaggi, A. Sani, "P-V equation of State, thermal expansion, and P-T stability of synthetic zincochromite ($ZnCr_2O_4$ spinel)", *Am. Mineral.*, vol. 90, pp. 1157-1162, 2005.

[26] S. Bordács, D. Varjas, I. Kézsmárki, G. Mihály, L. Baldassarre, A. Abouelsayed et al., "Magnetic-order-induced crystal symmetry lowering in ACr_2O_4 ferrimagnetic spinels", *Phys. Rev. Lett.*, vol. 103, pp. 077205, Aug. 2009.

[27] Ch. Kant, J. Deisenhofer, T. Rudolf, F. Mayr, F. Schrettle, A. Loidl et al., "Optical phonons, spin correlations, and spin-phonon coupling in the frustrated pyrochlore magnets $CdCr_2O_4$ and $ZnCr_2O_4$", *Phys. Rev. B*, vol. 80, pp. 214417, Dec. 2009.

[28] A. A. Khassin, G. N. Kustova, H. Jobic, T. M. Yurieva, Y. A. Chesalov, G. A. Filonenkoet al., "The state of absorbed hydrogen in the structure of reduced copper chromite from the vibration spectra The state of absorbed hydrogen in the structure of reduced copper chromite from the vibration spectra", *Phys. Chem. Chem. Phys.*, vol. 11, pp. 6090-6097, May 2009.

[29] J. B. Reddy and R. L. Frost, "Spectroscopic characterization of chromite from the Moa-Baracoa Ophiolitic Massif, Cuba", *Spectrochim. Acta Part A*, vol. 61, pp. 1721-1728, June 2005.

[30] D. P. Shoemaker and R. Seshadri, "Total-scattering descriptions of local and cooperative distortions in the oxide spinel $Mg_{1-x}Cu_xCr_2O_4$ with dilute Jahn-Teller ions", *Phys. Rev. B*, vol. 82, pp. 214107, Dec. 2010.

[31] M. M. Sinha, "Vibrational analysis of optical phonons in mixed chromite spinels", *Nucl. Instrum. Methods Phys. Res. Sect. B*, vol. 153, pp. 183-185, June1999.
[32] Z. V. Stanojević Marinković, N. Romčević, B. Stojanović, "Spectroscopic study of spinel $ZnCr_2O_4$ obtained from mechanically activated ZnO-Cr_2O_3 mixtures", *J. Eur. Ceram. Soc.*, vol. 27, pp. 903-907, 2007.
[33] Z. Wang, P. Lazor, S. K. Saxena, G. Artioli, "High-pressure Raman spectroscopic study of spinel ($ZnCr_2O_4$)", *J. Solid State Chem.*, vol. 165, pp. 165-170, Apr. 2002.
[34] Y. Yamasaki, S. Miyasaka, Y. Kaneko, J. P. He, T. Atime, Y. Tokura, "Magnetic reversal of the ferroelectric polarization in a multiferroic spinel oxide", *Phys. Rev. Lett.*, vol. 96, pp. 207204, May 2006.